Input Convex Kolmogorov Arnold Networks

Thomas Deschatre* Xavier Warin †

February 10, 2026

Abstract

This article presents an input convex neural network architecture using Kolmogorov-Arnold networks (ICKAN). Two specific networks are presented: the first is based on a low-order, piecewise-linear representation of functions, and a universal approximation theorem is provided. The second is based on cubic splines, for which only numerical results support convergence. We demonstrate through simple tests that these networks perform competitively with classical input convex neural networks (ICNNs). We then use the networks to solve optimal transport problems that require a convex approximation of functions and demonstrate their effectiveness. Cubic-ICKANs produce results similar to those of ICNNs.

1 Introduction

Recently, Kolmogorov-Arnold networks (KANs) have been introduced as an alternative to multilayer perceptrons for high-dimensional function approximation, based on the Arnold-Kolmogorov representation theorem [19]. Arnold and Kolmogorov demonstrated [14] that a multivariate continuous smooth $\mathbb{R}$ valued function f on a bounded domain can be expressed as a finite composition of sums of continuous single-variable functions. Specifically, if f is continuous on $[0,1]^n$, then

$$f(x) = \sum_{i=1}^{2n+1} \psi_i \left(\sum_{j=1}^{n} \Phi_{i,j}(x_j) \right), \tag{1}$$

where $\Phi_{i,j} : [0,1] \longrightarrow \mathbb{R}$ and $\psi_i : \mathbb{R} \longrightarrow \mathbb{R}$, $i = 1, \dots, 2n+1$, $j = 1, \dots, n$. Since the one-dimensional functions ψ and Φ can be highly irregular or even fractal, it has been demonstrated that they may not be practically learnable [12, 24]. To address this issue, Kůrková in [17, Theorem 1] proposed considering an approximate representation f_m instead of an exact one for a continuous function f, also extending the outer sum to m terms instead of $2n+1$, with m intended to be large and greater than $2n+1$. More recently, under the assumption that f is α-Hölder ($0 < \alpha \leq 1$) and also using m terms on the outer summation, [28] constructed an approximation f_m with $\Phi_{i,j}$ C^2 converging to f in the sup norm as m increases (see also [9] for another construction approximating the function in the sup norm). In this work, we follow the approach of [19]. Firstly, they suggest not restricting the outer sum in 1 to $2n+1$ terms but to m terms and define a KAN l^{th} layer, $l = 0, \dots, L$, as an operator $\psi^l_{m,q}$ from $[0,1]^m$ to $\mathbb{R}^q$:

$$(\psi^l_{m,q}(x))_k = \sum_{j=1}^{m} \Phi_{l,k,j}(x_j), \text{ for } k = 1, \dots, q. \tag{2}$$

*EDF R&D & FiME thomas.deschatre at edf.fr
†EDF R&D & FiME xavier.warin at edf.fr

Second, by stacking the layers, i.e., composing the operators ψ^l, $l = 0 \ldots, L$, they define the KAN operator from $[0,1]^m$ to $\mathbb{R}$:

$$K(x) = \psi^L_{n_{L-1},d} \circ \psi^{L-1}_{n_{L-2},n_{L-1}} \circ \ldots \circ \psi^1_{n_0,n_1} \circ \psi^0_{m,n_0}(x). \tag{3}$$

Since all functions $\Phi_{l,k,j}$ are one-dimensional, many classical numerical techniques are available to construct implementable approximations. The implementation proposed in [19] uses B-splines and is numerically costly, but other approximations based on wavelets [4], radial basis functions [18, 29], and Chebyshev polynomials [27] have been introduced to reduce computation time.

All these representations share the same limitation: the output of a layer may not lie on the grid originally chosen for the next layer. Mapping the output, a priori in $\mathbb{R}^q$, back to $[0,1]^q$ using, for example, a sigmoid function is possible, but this typically reduces the accuracy and slows convergence. Although [19] propose an adaptation technique, it fails numerically. Recently, using a P1 finite-element formulation, [34] introduced a new P1-KAN architecture that avoids this issue and established its convergence; numerical examples on function approximation using a mean squared error (MSE) criterion and real applications such as hydraulic valley optimization show that P1-KAN is more efficient than MLPs and all tested KAN variants.

In this article, we extend the work of [34] and propose new architectures to approximate convex functions using convex approximations. Convexity is essential in many applications. For instance, in optimal transport, the optimal transport map is the gradient of a convex function (Brenier's theorem [5]). Similarly, in optimal control, the value function may be convex or concave. For example, in gas storage optimization, it is crucial for practitioners to preserve the concavity of the Bellman value with respect to the stock level; the marginal cost, defined as the derivative of this Bellman value, must decrease as the stock level increases.

The approximation of a convex function while preserving convexity has been widely studied. Approximation by cuts using regression has been explored in [3, 10, 11, 13], leading to max-affine approximations. A max-affine representation using group-max neural networks [33] has been proposed and proved convergent, relying on the fact that a convex function can be ϵ-approximated by the maximum of finitely many affine functions. Other theoretical results appear in [6], which uses a one-layer feedforward network with exponential activations inside and a log-sum-exp output, a standard convex function. Numerically, [2] introduced input convex neural networks (ICNNs), whose convergence was proved in [7]; ICNNs have since been used in many convex-approximation contexts, such as optimal transport [20, 15], optimal control [7, 1], inverse problems [23], and general optimization [8]. Input-convex KANs have also been tested for modeling hyperelastic materials [30], independently of our work.

We propose two Kolmogorov–Arnold architectures:

- The first version uses a piecewise linear approximation of the 1D functions in the KAN representation. It is based on the P1-KAN network of [34]. Unlike other KAN architectures, it takes as input a grid G^1 defining the approximation domain and outputs both the function value and a grid G^2 representing the image of G^1. This explicit definition facilitates layer composition. By enforcing convexity in the 1D approximation, we develop a new network and provide a Universal Approximation Theorem.

- The second version uses a Hermite cubic spline approximation, also enforcing convexity. This network provides a higher-order approximation, which is desirable when the gradient of the convex function is of interest. In such cases, a piecewise linear approximation produces only piecewise-constant gradients, which may be insufficient. However, no convergence guarantees are established.

In 2, we describe the two networks in the class of input convex Kolmogorov–Arnold networks (ICKANs), giving both the adapted and non-adapted grid versions (as in [34]). We compare these variants under a mean squared error criterion and show that their performance is comparable to ICNNs. In 3, we extend

these networks to the case in which the function is convex only with respect to part of the input, yielding partial input convex Kolmogorov–Arnold networks (PICKANs). We compare their performance with the corresponding partial ICNNs (PICNNs). Finally, in 4, we use ICKANs to compute optimal transport maps between two distributions on simulated data, illustrating the efficiency of the proposed networks.

2 ICKAN

We assume throughout this section that the target function is fully convex. In the first part, we explain how to construct a one-dimensional convex approximation of a function on $[0,1]$, either using a piecewise-linear representation or a cubic-spline one. In the second part, we detail the construction of the layers associated with the two proposed networks and we establish a Universal Approximation Theorem for the first architecture. In the third part, we present several numerical experiments.

2.1 Approximation of a 1D convex function f on $[0,1]$

We introduce the lattice $\{\hat{x}_0 := 0\} \cup (\hat{x}_p)_{1\leq p\leq P-1} \cup \{\hat{x}_P := 1\}$ where the points $\hat{x}_p \in [0,1]$ form an increasing sequence indexed by p.

2.1.1 Piecewise linear approximation

For $P > 0$, the degrees of freedom of a $P1$ approximation ϕ of f are the values of the function on the lattice leading to

$$\phi(x) = \sum_{p=0}^{P} a_p \Psi_p(x) \tag{4}$$

where $(a_p)_{p=0,\dots,P}$ are approximations of $(f(\hat{x}_p))_{p=0,\dots,P}$ and $(\Psi_p)_{p=0,\dots,P}$ is the basis of the shape functions: these functions have compact support in each interval $[\hat{x}_{p-1}, \hat{x}_{p+1}]$ for $p = 1,\dots,P-1$ and are defined as:

$$\Psi_p(x) = \begin{cases} \frac{x-\hat{x}_{p-1}}{\hat{x}_p-\hat{x}_{p-1}} & \text{for } x \in [\hat{x}_{p-1}, \hat{x}_p], \\ \frac{\hat{x}_{p+1}-x}{\hat{x}_{p+1}-\hat{x}_p} & \text{for } x \in [\hat{x}_p, \hat{x}_{p+1}], \end{cases} \tag{5}$$

for $p = 1,\dots,P-1$ and $\Psi_0(x) = \max(1 - \frac{x-\hat{x}_0}{\hat{x}_1-\hat{x}_0}, 0)$, $\Psi_P(x) = \max(\frac{x-\hat{x}_{P-1}}{\hat{x}_P-\hat{x}_{P-1}}, 0)$ (see 1). Since we seek a convex function, the piecewise-linear approximation must have non-decreasing derivatives on each mesh interval $[\hat{x}_p, \hat{x}_{p+1}]$ for $p = 0,\dots,P-1$. The trainable variables of the convex approximation are b, an approximation of $f(0)$, $\hat{b}$, an approximation of $f'(0)$, and $(d_i)_{i=1,\dots,P-1}$ an approximation of $f'(\hat{x}_i) - f'(\hat{x}_{i-1})$ for $i = 1,\dots,P$.
Therefore $a_p \approx f(\hat{x}_p)$ in 4 is given by:

$$a_p = b + \sum_{j=1}^{p} \Big(\hat{b} + \sum_{i=1}^{j-1} \max(d_i, 0)\Big) (\hat{x}_j - \hat{x}_{j-1}), \; p = 0,\dots,P, \tag{6}$$

where the max is here to ensure that the approximation $f'(\hat{x}_p) \approx \hat{b} + \sum_{i=1}^{p} \max(d_i, 0)$ is non-decreasing in p. It is also possible to adapt the grid, following [34]. In that case, the interior vertices in $]0,1[$ are initialized uniformly at random and trained to adapt to the data. This is achieved by defining, for $1 \leq p < P$,

$$\hat{x}_p = \frac{\sum_{k=1}^{p} e_k}{\sum_{k=1}^{P} e_k}, \tag{7}$$

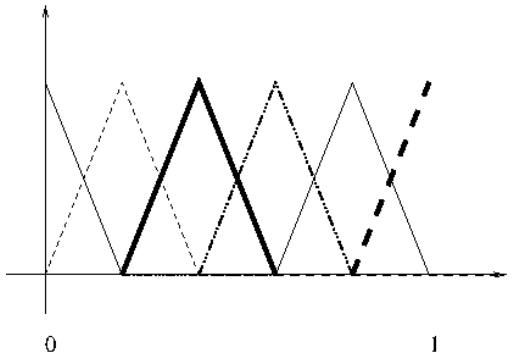

Figure 1: Uniform P1 basis functions on $[0, 1]$ with $P = 5$.

where $e_1, \ldots, e_P$ are positive variables. Thus, b, $\hat{b}$, $(d_i)_{i=1,\ldots,P-1}$ and $(e_i)_{i=1,\ldots,P}$ are learned during training. In A.1, we demonstrate the effect of adaptation on the P1-ICKAN.

2.1.2 The cubic approximation

On a mesh interval $[\hat{x}_p, \hat{x}_{p+1}]$, the function f is approximated for $x \in [\hat{x}_p, \hat{x}_{p+1}]$ using a cubic Hermite spline of the form $\phi_p\left(\frac{x-\hat{x}_p}{\hat{x}_{p+1}-\hat{x}_p}\right)$ where:

$$\begin{aligned}\phi_p(t) =& f(\hat{x}_p)h_{00}(t) + f'(\hat{x}_p)h_{10}(t)(\hat{x}_{p+1} - \hat{x}_p)\\ &+ f(\hat{x}_{p+1})h_{01}(t) + f'(\hat{x}_{p+1})h_{11}(t)(\hat{x}_{p+1} - \hat{x}_p)\end{aligned}$$

and the cubic Hermite basis functions are given by

$$\begin{aligned}h_{00}(t) =& 2t^3 - 3t^2 + 1,\\ h_{10}(t) =& t^3 - 2t^2 + t,\\ h_{01}(t) =& -2t^3 + 3t^2,\\ h_{11}(t) =& t^3 - t^2.\end{aligned}$$

As before, we require the derivatives to be non-decreasing. Under this condition, the values $(f(\hat{x}_p))_{p=0,\ldots,P}$ must satisfy, for $p = 0, \ldots, P-1$,

$$\begin{aligned}f(\hat{x}_p) + \frac{\hat{x}_{p+1} - \hat{x}_p}{3}\Big(2f'(\hat{x}_p) + f'(\hat{x}_{p+1})\Big) \le f(\hat{x}_{p+1}),\\ f(\hat{x}_{p+1}) \le f(\hat{x}_p) + \frac{\hat{x}_{p+1} - \hat{x}_p}{3}\Big(f'(\hat{x}_p) + 2f'(\hat{x}_{p+1})\Big).\end{aligned}$$

Therefore the convex cubic-spline approximation on each mesh interval $[\hat{x}_p, \hat{x}_{p+1}]$ for $p = 0, \ldots, P-1$ is given by $\phi_p\left(\frac{x-\hat{x}_p}{\hat{x}_{p+1}-\hat{x}_p}\right)$ with

$$\phi_p(t) = a_p^0 h_{00}(t) + a_p^1 h_{10}(t)(\hat{x}_{p+1} - \hat{x}_p) + a_{p+1}^0 h_{01}(t) + a_{p+1}^1 h_{11}(t)(\hat{x}_{p+1} - \hat{x}_p), \tag{8}$$

where :

$$
\begin{aligned}
a_p^1 =& \hat{b} + \sum_{i=1}^{p} \max(d_i, 0), \\
a_p^0 =& b + \sum_{i=1}^{p} \frac{\hat{x}_i - \hat{x}_{i-1}}{3} \Big(2a_{i-1}^1 + a_i^1 + \sigma(g_i)(a_i^1 - a_{i-1}^1) \Big),
\end{aligned}
\tag{9}
$$

σ denotes the sigmoid function, and the parameters $\hat{b}, b, (d_i)_{i=1,\dots,P}, (g_i)_{i=1,\dots,P}$ are trainable. In the adapted version, the variables $(e_i)_{i=1,\dots,P}$ determining the grid positions $(\hat{x}_p)_{p=1,\dots,P-1}$ are also trained, exactly as in the piecewise-linear case. In A.2, we demonstrate the effects of adapting Cubic-ICKAN and optimising one layer.

2.2 The ICKAN layers

As in the P1–KAN architecture, an ICKAN layer takes as input a hypercube defining the domain together with the batched values x, and outputs both an estimate of the function at x and a hypercube representing the image of the original domain. This structure ensures that the layers can be composed in a consistent manner.

2.2.1 The P1-ICKAN layers

For the first component of the first layer, we define $\hat{\kappa}_{n,m}^0$ for $x \in [0,1]^n$ and the hypercube $G^0 := [0,1]^n$ as:

$$
\begin{aligned}
&\hat{\kappa}_{n,m}^0(x, G^0)_k = \\
&\quad \sum_{j=1}^{n} \sum_{p=0}^{P} \Bigg(b_{0,k,j} + \sum_{s=1}^{p} \Big(\hat{b}_{0,k,j} + \sum_{i=1}^{s-1} \max(d_{0,k,j,i}, 0) \Big) (\hat{x}_{0,j,s} - \hat{x}_{0,j,s-1}) \Bigg) \Psi_p^{0,j}(x_j), \\
&\quad \text{for } k = 1, \dots, m.
\end{aligned}
\tag{10}
$$

The values $(\hat{x}_{0,j,s})_{s=0,\dots,P}$ denote the one-dimensional grid for the j^{th} dimension of G^0, and $\Psi_p^{0,j}$ for $p = 1, \dots, P$ are the shape functions defined in 5 and shown in 1.

The image $G^1 = \prod_{k=1}^{m} [\underline{G}_k^1, \bar{G}_k^1]$ of G^0 by $\hat{\kappa}_{n,m}^0$ is exactly given by:

$$
\begin{aligned}
\underline{G}_k^1 =& \sum_{j=1}^{n} \min_{0 \le p \le P} \left[b_{0,k,j} + \sum_{s=1}^{p} \Big(\hat{b}_{0,k,j} + \sum_{i=1}^{s-1} \max(d_{0,k,j,i}, 0) \Big) (\hat{x}_{0,j,s} - \hat{x}_{0,j,s-1}) \right] \\
\bar{G}_k^1 =& \sum_{j=1}^{n} \max \left[b_{0,k,j}, b_{0,k,j} + \sum_{s=1}^{P} \Big(\hat{b}_{0,k,j} + \sum_{i=1}^{s-1} \max(d_{0,k,j,i}, 0) \Big) (\hat{x}_{0,j,s} - \hat{x}_{0,j,s-1}) \right]
\end{aligned}
\tag{11}
$$

for $1 \le k \le m$. Thus, the layer output is defined as

$$
\kappa_{n,m}^0(x, G^0) = (\hat{\kappa}_{n,m}^0(x, G^0), G^1). \tag{12}
$$

remark 2.1 *Since the approximation is convex, the maximum $\bar{G}_k^1$ is attained on the boundary of the domain.*

As a sum of convex one-dimensional functions in each coordinate, $\hat{\kappa}^0_{n,m}(\cdot, G^0)$ has a diagonal, positive-definite Hessian.

To ensure convexity is preserved through composition, we require each subsequent layer $\hat{\kappa}^l_{m,q}(x, G^l)$ $(l \geq 1)$ to be convex and non-decreasing in x as in [2]. It suffices to impose $\hat{b}_{l,k,j} \geq 0$ for all k and j. Thus, for $l \geq 1$, with G^l the input hypercube, we define

$$\begin{aligned}&\hat{\kappa}^l_{m,q}(x, G^l)_k = \\ &\sum_{j=1}^{m}\sum_{p=0}^{P}\Bigg(b_{l,k,j} + \sum_{s=1}^{p}\Big(\max(\hat{b}_{l,k,j}, 0) + \sum_{i=1}^{s-1}\max(d_{l,k,j,i}, 0)\Big)(\hat{x}_{l,j,s} - \hat{x}_{l,j,s-1})\Bigg)\Psi_p^{l,j}(x_j), \\ &\text{for } k = 1, \ldots, q,\end{aligned}$$

and the output hypercube G^{l+1} image of G^l is defined analogously to 11. The complete layer is then defined as

$$\kappa^l_{m,q}(x, G^l) = (\hat{\kappa}^l_{m,q}(x, G^l), G^{l+1}). \tag{13}$$

By concatenating L layers, and denoting n_l the number of neurons in layer l (as in 3), assuming the number of mesh points P is fixed across neurons, we define the full network:

$$K(x) = \hat{\kappa}^L_{n_{L-1},1} \circ \kappa^{L-1}_{n_{L-2},n_{L-1}} \circ \ldots \circ \kappa^0_{n,n_0}(x, [0,1]^n). \tag{14}$$

As in [34], we propose two variants:

- **Uniform grid.** The mesh is fixed, and the trainable parameters are

$$\begin{aligned}\mathcal{A} :=&(b_{0,k,j}, \hat{b}_{0,k,j}, (d_{0,k,j,i})_{i=1,\ldots,P-1})_{k=1,\ldots,n_0,j=0,\ldots,n} \cup \\ &(b_{l,k,j}, \hat{b}_{l,k,j}, (d_{l,k,j,i})_{i=1,\ldots,P-1})_{l=1,\ldots,L-1,k=1,\ldots,n_l,j=0,\ldots,n_{l-1}} \cup \\ &(b_{L,1,j}, \hat{b}_{L,1,j}, (d_{L,1,j,i})_{i=1,\ldots,P-1})_{j=0,\ldots,n_{L-1}}.\end{aligned}$$

- **Adaptive grid.** In addition to $\mathcal{A}$, the interior grid points are trainable, i.e.

$$\mathcal{A} \cup (e_{0,j,p})_{j=1,\ldots,n,p=1,\ldots,P} \cup (e_{l,j,p})_{l=1,\ldots,L,j=1,\ldots,n_l,p=1,\ldots,P}$$

  where the variables $e_{l,j,p}$ determine the grid values $\hat{x}_{l,j,p}$ via a formula similar to 7.

2.2.2 The Cubic-ICKAN layers

Consider again the one-dimensional lattice $(\hat{x}_{0,j,s})_{s=0,\ldots,P}$ on $G^0 := [0,1]^n$ associated with the jth input dimension. We define $\hat{\kappa}^0_{n,m}$ for

$$x \in \prod_{j=1}^{n}[\hat{x}_{0,j,p_j}, \hat{x}_{0,j,p_j+1}], \qquad p_j \in \{0, \ldots, P-1\},\ j = 1, \ldots, n,$$

and for the hypercube G^0 by

$$\begin{aligned}\hat{\kappa}^0_{n,m}(x, G^0)_k =& \sum_{j=1}^{n} a^0_{0,j,p_j} h_{00}(t_{0,j}) + a^1_{0,j,p_j} h_{10}(t_{0,j})(\hat{x}_{0,j,p_j+1} - \hat{x}_{0,j,p_j}) \\ &+ a^0_{0,j,p_j+1} h_{01}(t_{0,j}) + a^1_{0,j,p_j+1} h_{11}(t_{0,j})(\hat{x}_{0,j,p_j+1} - \hat{x}_{0,j,p_j}), \\ &\text{for } k = 1, \ldots, m,\end{aligned} \tag{15}$$

where $t_{0,j} = \frac{x_j - \hat{x}_{0,j,p_j}}{\hat{x}_{0,j,p_j+1} - \hat{x}_{0,j,p_j}}$,

$$\begin{aligned} a^1_{0,j,p_j} &= \hat{b}_{0,j} + \sum_{i=1}^{p_j} \max(d_{0,j,i}, 0), \\ a^0_{0,j,p_j} &= b_{0,j} + \sum_{i=1}^{p_j} \frac{\hat{x}_{0,j,i} - \hat{x}_{0,j,i-1}}{3} \left(2a^1_{0,j,i} + a^1_{0,j,i-1} + \sigma(g_{0,j,i})(a^1_{0,j,i} - a^1_{0,j,i-1})\right). \end{aligned} \tag{16}$$

The image hypercube $G^1 = \prod_{k=1}^{m} [\underline{G}^1_k, \bar{G}^1_k]$ is defined by

$$\begin{aligned} \underline{G}^1_k &= \sum_{j=1}^{n} \min_{0 \le p \le P} a^0_{0,j,p} \\ \bar{G}^1_k &= \sum_{j=1}^{d_0} \max\left[a^0_{0,j,0}, a^0_{0,j,P}\right]. \end{aligned} \tag{17}$$

Note that G^1 is itself included in the image of G^0 under $\hat{\kappa}^0_{n,m}$.

To ensure that G^1 coincides exactly with the image of the layer, we may truncate the output:

$$\kappa^0_{n,m}(x, G^0) = \left(\left(\max\left(\hat{\kappa}^0_{n,m}(x, G^0)_k, \underline{G}^1_k\right)\right)_{k=1,\dots,m}, G^1\right).$$

remark 2.2 *Due to convexity, only the minimum value needs to be truncated. Clipping the value function reveals the effective image of the layer, which can then be used as the domain for the next layer. Semi-Lagrangian schemes in control problems also perform clipping inside interpolations, yielding nearly monotone schemes with provable convergence rates [32]. In practice, the original KAN architecture does not adjust its grid to the output domain and still performs well; numerically, the effect of the truncation here is small.*

Similarly to the piecewise linear case, for $l \ge 1$, G^l being the hypercube defining the domain, the operator $\hat{\kappa}^l_{m,q}(x, G^l)_k$ for $l \ge 1$ is defined similarly to 15 using

$$a^1_{l,j,p_j} = \max(\hat{b}_{l,j}, 0) + \sum_{i=1}^{p_j} \max(d_{l,j,i}, 0)$$

instead of 16. The output hypercube G^{l+1} image of G^l is given by an expression similar to 17. Then the layer is defined by:

$$\kappa^l_{m,q}(x, G^l) = \left(\left(\max\left(\hat{\kappa}^l_{m,q}(x, G^l)_k, \underline{G}^{l+1}_k\right)\right)_{k=1,\dots,q}, G^{l+1}\right).$$

The concatenation of layers is still defined by 14. As in the piecewise-linear case, one may use either a uniform grid or an adaptive grid.

2.2.3 Convergence results

We provide two universal approximation theorems in the piecewise-linear setting, corresponding to the adapted and non-adapted cases.

Theorem 2.1 *The space spanned by the P1-ICKAN allowing n_l for $l = 0, \ldots, L-1$ and L to vary for $P > 1$ is dense in the set of Lipschitz convex functions on $[0,1]^n$ with respect to the sup norm when adaptation is used.*

The proof of 2.1 is given in B.1. We also establish a theorem for the non-adapted case; the proof is provided in B.2.

Theorem 2.2 *The space spanned by the P1-ICKAN allowing n_l for $l = 0, \ldots, L-1$, L and P to vary is dense in set of Lipschitz convex functions on $[0,1]^n$ with respect to the sup norm when no adaptation is used.*

2.2.4 Numerical Results

In this section, we compare the performance of the proposed networks with that of the ICNN. We first study their approximation capabilities on a d-dimensional convex function, and then examine a two-dimensional toy control example.

Numerical approximation We estimate the function

$$f(x) = \sum_{i=1}^{d} (|x_i| + |1 - x_i|) + x^\top A x \tag{18}$$

where A is a positive-definite matrix, using both an input convex neural network with ReLU activation and an input convex Kolmogorov network approximation $\tilde{f}^\theta$ parametrized by θ. The approximation is obtained by minimizing the empirical version of

$$\mathbb{E}[(f(X) - \tilde{f}^\theta(X))^2] \tag{19}$$

where $X \sim U[-2,2]^d$. We use the ADAM optimizer with a learning rate of 10^{-3}, a batch size of 1,000, and perform 200,000 iterations. Based on 10 independent runs, we compute the average MSE and its standard deviation on a validation batch of size 100,000 for different parameter choices.

For the ICNN, we consider networks with 2, 3, 4, or 5 layers, with a number of neurons chosen from $\{10, 20, 40, 80, 160, 320\}$, and ReLU activation. Among all tested configurations, the ICNN yielding the smallest average MSE is selected as the reference model.

Results for dimensions 3 and 7 are reported in **??**. For the P1–ICKAN, the performance is stable across values of P and across the number of layers. The adaptive version (P1–ICKAN adapt) performs better than the non-adaptive one. In dimension 3, the adaptive P1–ICKAN achieves accuracy comparable to the best ICNN, while in dimension 7 it outperforms the ICNN, despite having significantly fewer parameters.

Interestingly, the computational cost is almost independent of P and of the problem dimension, thanks to efficient GPU parallelization. Although the P1–ICKAN uses fewer parameters than a feedforward network of comparable accuracy, the computational time is typically three to four times larger.

In 3, results in dimension 7 using the Cubic-ICKAN show that the approximation is good but at a computational cost much higher than the P1-ICKAN.

We may wonder what happens if we incorrectly assume that the function to be learned is convex. We consider

$$f(x) = A + 2\mathbf{1}_d^\top x + x^\top Q x, \tag{20}$$

where $Q = -0.5$ if $d = 1$, $Q = \begin{pmatrix} 1 & 0 \\ 0 & -0.5 \end{pmatrix}$ if $d = 2$, $\mathbf{1}_d$ the vector of dimension d with all components equal to 1 and $A = 1$. 2 shows the reference function and its approximation for the case $d = 1$ while 3 shows the

Table 1: Results over 10 runs for the minimization of 19 in dimension 3 for the function in 18 : ICCN versus P1-ICKAN. *NBL* stands for the number of layers, *NBN* the number of neurons, *nbParam* the number of model parameters, while *Time* stands for the time in seconds for one hundred iterations of the stochastic gradient descent.

method	NBL	NBN	P	Average	std	nbParam	Time
Best ICNN	2	320		9.37E-05	8.29E-05	105284	0.14
P1-ICKAN	2	20	20	1.56E-04	7.39E-05	10080	0.54
P1-ICKAN	2	20	40	1.14E-04	9.79E-05	19680	0.54
P1-ICKAN	2	40	20	2.62E-04	3.68E-04	36960	0.55
P1-ICKAN	2	40	40	2.69E-04	4.65E-04	72160	0.53
P1-ICKAN	3	20	20	3.13E-04	3.10E-04	18480	0.73
P1-ICKAN	3	20	40	6.83E-04	1.04E-03	36080	0.73
P1-ICKAN	3	40	20	2.76E-04	1.90E-04	70560	0.73
P1-ICKAN	3	40	40	1.67E-04	2.91E-04	137760	0.73
P1-ICKAN adapt	2	20	20	1.23E-04	4.62E-05	10940	0.66
P1-ICKAN adapt	2	20	40	1.93E-04	3.72E-04	21400	0.66
P1-ICKAN adapt	2	40	20	2.62E-04	2.97E-04	38620	0.66
P1-ICKAN adapt	2	40	40	1.13E-04	1.42E-04	75480	0.66
P1-ICKAN adapt	3	20	20	9.82E-04	2.23E-03	19740	0.88
P1-ICKAN adapt	3	20	40	1.93E-04	2.75E-04	38600	0.88
P1-ICKAN adapt	3	40	20	3.63E-04	6.50E-04	73020	0.88
P1-ICKAN adapt	3	40	40	5.35E-04	1.16E-03	142680	0.88

Table 2: Results over 10 runs for the minimization of 19 in dimension 7 for function in 18: ICCN versus P1-ICKAN. *NBL* stands for the number of layers, *NBN* the number of neurons, *nbParam* the number of model parameters, while *Time* stands for the time in seconds for one hundred iterations of the stochastic gradient descent.

method	NBL	NBN	P	Average	std	nbParam	Time
Best ICNN	2	320		2.39E-03	6.72E-04	107848	0.14
P1-ICKAN	2	40	10	8.19E-03	9.23E-04	21120	0.54
P1-ICKAN	2	40	20	3.71E-03	4.69E-03	40320	0.54
P1-ICKAN	2	40	40	1.94E-03	1.20E-03	78720	0.53
P1-ICKAN	3	40	10	9.05E-03	1.25E-03	38720	0.73
P1-ICKAN	3	40	20	2.40E-03	8.88E-04	73920	0.73
P1-ICKAN	3	40	40	3.45E-03	2.09E-03	144320	0.73
P1-ICKAN adapt	2	40	10	2.31E-03	6.88E-04	21990	0.66
P1-ICKAN adapt	2	40	20	2.72E-03	2.95E-03	42060	0.67
P1-ICKAN adapt	2	40	40	1.33E-03	1.03E-03	82200	0.67
P1-ICKAN adapt	3	40	10	2.69E-03	1.08E-03	39990	0.88
P1-ICKAN adapt	3	40	20	2.87E-03	1.89E-03	76460	0.89
P1-ICKAN adapt	3	40	40	2.24E-03	2.47E-03	149400	0.89

Table 3: Results over 10 runs for the minimization of 19 in dimension 7 for function in 18: ICCN versus Cubic-ICKAN (C-ICKAN). *NBL* stands for the number of layers, *NBN* the number of neurons, *nbParam* the number of model parameters, while *Time* stands for the time in seconds for one hundred iterations of the stochastic gradient descent.

method	NBL	NBN	P	Average	std	nbParam	Time
Best ICNN	2	320		2.39E-03	6.72E-04	107848	0.14
C-ICKAN	2	20	10	6.66E-03	2.06E-03	12320	1.32
C-ICKAN	2	20	20	3.59E-03	7.64E-04	23520	1.31
C-ICKAN	2	40	10	3.88E-03	1.06E-03	42240	1.47
C-ICKAN	3	20	10	6.19E-03	2.11E-03	21120	1.79
C-ICKAN	3	20	20	5.04E-03	2.81E-03	40320	1.79
C-ICKAN	3	40	10	3.82E-03	1.64E-03	77440	2.03
C-ICKAN adapt	2	20	10	1.43E-03	6.29E-04	12790	1.49
C-ICKAN adapt	2	20	20	1.19E-03	8.76E-04	24460	1.55
C-ICKAN adapt	2	40	10	1.38E-03	1.28E-03	43110	1.65
C-ICKAN adapt	3	20	10	3.06E-03	1.66E-03	21790	2.06
C-ICKAN adapt	3	20	20	1.95E-03	1.43E-03	41660	2.07
C-ICKAN adapt	3	40	10	1.49E-03	1.11E-03	78710	2.23

error as the difference between the real function and its approximation for the case $d = 2$: it shows that the error is concentrated on the axis supporting the non-convexity. The quadratic shape of the error indicates that the network is clipping the negative eigenvalues of the hessian matrix.

A toy control example in dimension 2 We consider the simple linear quadratic problem with dynamics

$$x_{t+1} = Ax_t + Bu_t + w_t,\ t = 0, \dots, N-1,$$

where $(x_t, u_t, w_t) \in \mathbb{R}^2 \times \mathbb{R}^2 \times \mathbb{R}^2$, $(w_t)_{t=0,\dots,N-1}$ are i.i.d. centered Gaussian noises with covariance matrix $W \in \mathbb{R}^{2\times 2}$ and x_0 is given . The control is chosen in feedback form $u_t = \phi_t(x_t)$ before observing the noise. The matrices $A, B \in \mathbb{R}^{2\times 2}$ are given. The objective is to minimize

$$J(x_0, (u_t)_{t=0,\dots,N-1}) = \mathbb{E}\Big[\sum_{t=0}^{N-1} \Big(x_t^\top Q x_t + u_t^\top R u_t\Big) + x_N^\top Q_f x_N | x_0\Big]$$

where Q and R are two positive semi-definite two-dimensional matrices.
The optimal control u_t^* associated the optimal trajectory x_t^* is given by

$$\begin{aligned} u_t^* = \phi_t(x_t) =& K_t {x_t}^*, \\ K_t =& -(B^\top P_{t+1} B + R)^{-1} B^\top P_{t+1} A, \end{aligned}$$

where the backward Riccati recursion is

$$\begin{aligned} P_t =& A^\top P_{t+1} A - A^\top P_{t+1} B (B^\top P_{t+1} B + R)^{-1} B^\top P_{t+1} A + Q \\ P_N =& Q_f \end{aligned}$$

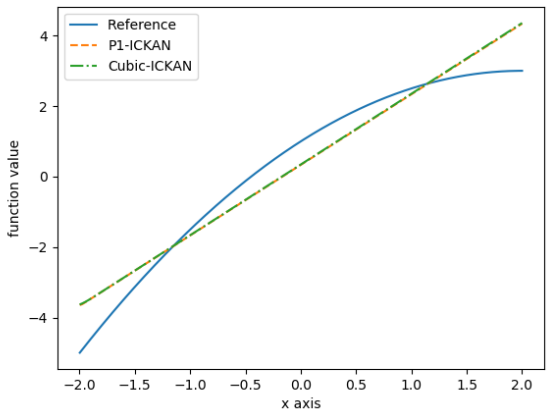

Figure 2: Estimation of the function in 20 for dimension $d = 1$ wrongly supposing that the function is convex, network with $P = 10$.

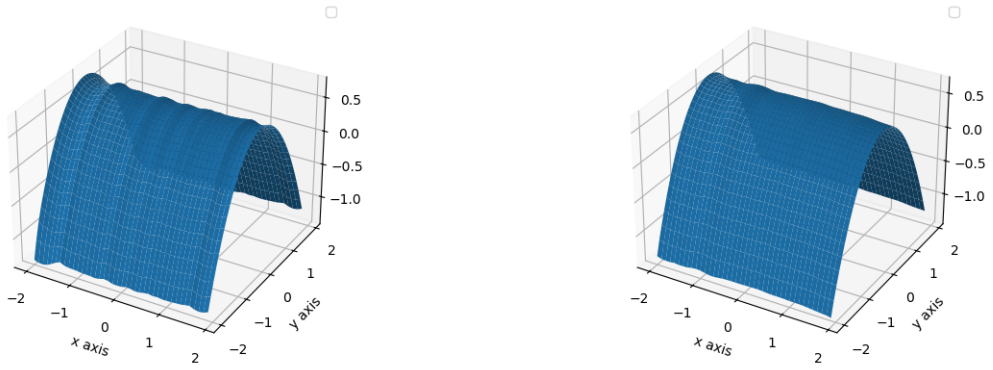

P1-ICKAN Cubic-ICKAN

Figure 3: Error for the function in 20 for dimension $d = 2$ wrongly supposing that the function is convex, network with $P = 10$.

and the optimal cost function J^* satisfies $J^*(x_0) = x_0^\top P_0 x_0 + r_0$ with

$$\begin{aligned} r_t =& r_{t+1} + \mathrm{Tr}\left[W P_{t+1}\right] \\ r_N =& 0. \end{aligned}$$

We assume that the optimal control u_t^* is known exactly, and our goal is to approximate the convex value function J^* on $[-3,3]^2$. Applying the optimal control to trajectories generated from a sample of $(w_t)_{t=0,\dots,N-1}$ and $x_0 \sim U([-3,3]^2)$ yields the cost

$$C(x_0, (w_t)_{t=0,\dots,N-1}) = \sum_{t=0}^{N-1} \Big((x_t)^\top Q x_t + (K_t x_t)^\top R (K_t x_t) \Big) + x_N^\top Q_f x_N.$$

Using a convex neural network κ^θ parametrized by θ to approximate J^*, we minimize

$$L(\theta) = \mathbb{E}[(\kappa^\theta(x_0) - C(x_0, (w_t)_{t=0,\dots,N-1}))^2] \tag{21}$$

We choose $Q = R = A = B = Q_f = W = \begin{pmatrix} 1 & 0 \\ 0 & 1 \end{pmatrix}$ for our test case. The optimizer settings are the same as in the previous experiment. For the ICNN, we use three hidden layers with 30 neurons. For the ICKAN, we use two hidden layers with 10 neurons and a mesh size $P = 10$. One hundred iterations of stochastic gradient descent require 0.29 seconds for the ICNN, 0.69 seconds for the P1-ICKAN, and 1.14 seconds for the Cubic-ICKAN.

4 displays the relative errors obtained by the three networks. The maximal error is reduced by nearly a factor of two when using convex KAN architectures compared with ICNN. As expected, the cubic version yields a smoother approximation.

3 PICKAN

We assume in this section that the function f to be approximated is partially convex: $f(x,y)$ is convex in $y \in \mathbb{R}^{n_y}$ but not necessarily convex in $x \in \mathbb{R}^{n_x}$. We assume that the function is defined on $G^0 = G_x^0 \times G_y^0$, where $G_x^0 = [0,1]^{n_x}$ and $G_y^0 = [0,1]^{n_y}$.

We present the network architecture using a piecewise-linear approximation of the one-dimensional functions, although the same construction can be adapted to a cubic-spline approximation.

We denote by P1–KANL the layer structure introduced in [34], and by $\rho_{p,q}^l$ the corresponding operator for layer l with input dimension p and output dimension q. The first layer κ^0, defined in 12, is denoted ICKANL0, while any layer κ^l with $l > 0$, defined in 13, is denoted ICKANL1.

The architecture of the network is illustrated in 5. The recursion described in 5 is given for $M > 0$ by:

$$\begin{aligned} (X_1, G_x^1) =& \rho_{n_x,M}^0(x, G_x^0), \\ (Y_1, G_y^1) =& (X_1, G_x^1) + \kappa_{n_y,M}^0(y, G_y^0), \\ (X_{i+1}, G_x^{i+1}) =& \rho_{M,M}^i(X_i, G_x^i), \\ (Y_{i+1}, G_y^{i+1}) =& (X_{i+1}, G_x^{i+1}) + \kappa_{M,M}^i(Y_i, G_y^i) \quad \text{for } i = 1, L-1, \\ (Y_{L+1}, G_y^{L+1}) =& \kappa_{M,1}^L(Y_L, G_y^L). \end{aligned}$$

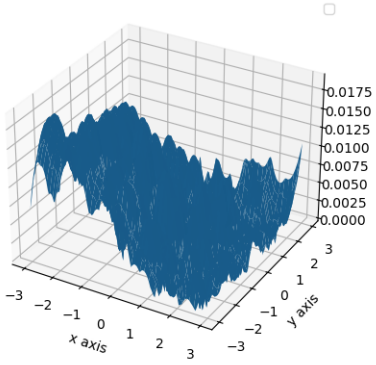

ICNN

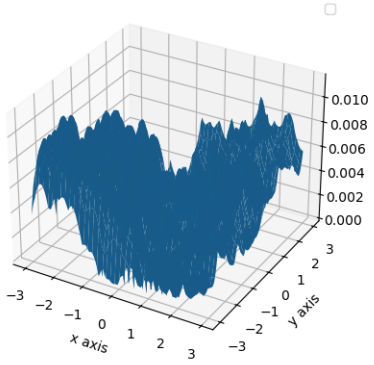

P1-ICKAN

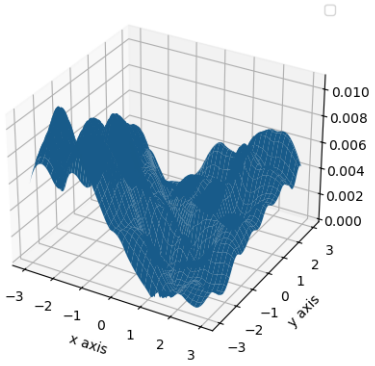

Cubic-ICKAN

Figure 4: Relative error given by 21 obtained on the linear quadratic optimal control problem.

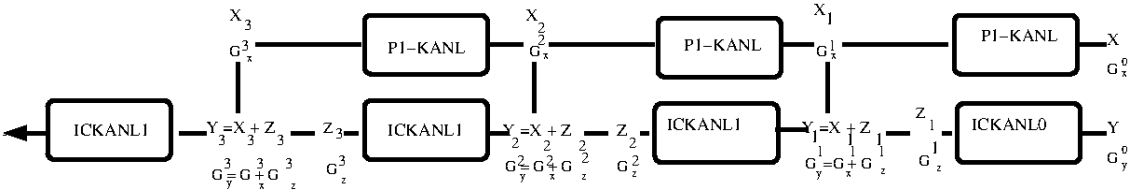

Figure 5: Partial input convex Kolmogorov Arnold network using a piecewise linear approximation.

remark 3.1 *When f is non-convex, setting $\kappa^0_{n_y,M} = 0$, $\kappa^l_{M,M} = 0$ for $1 < l < L$ and $\kappa^L_{M,1}(x) = x_1$ recovers the P1–KAN architecture, which is known to converge when the Kolmogorov–Arnold basis functions are Lipschitz. When the function f is convex, forcing the P1–KANL outputs to vanish recovers the ICKAN network.*

remark 3.2 *In the PICKAN architecture, the contributions from the convex and non-convex parts are added together, in the same manner as in the Kolmogorov–Arnold layer (2).*

remark 3.3 *Depending on the regularity of the function in x and in y, one may use different approximation orders in each variable.*

remark 3.4 *The PICKAN model introduced here belongs to the class of parametrized convex functions studied in [25]. However, the architecture depicted in 5 differs from that of Schaller et al.: they consider a feedforward neural network whose weights and biases depend on y, with a nondecreasing convex activation function and nonnegative weights, while also taking x as an input at each layer.*

We estimate the function

$$f(x, y) = |y + 1||x + 2x^3| \text{ on } [-2, 2]^2, \tag{22}$$

by minimizing the empirical version of

$$\mathbb{E}[(f(X, Y) - \tilde{f}^\theta(X, Y))^2],$$

where $\tilde{f}^\theta$ is our neural network approximation parametrized by θ and $(X, Y) \sim U[-2, 2]^2$. As before, we use the ADAM optimizer with 200,000 iterations and learning rate 10^{-3}. For the ICNN with ReLU activation, we test architectures with 2, 3, or 4 layers, and hidden sizes in $\{10, 20, 40, 80, 160\}$. For each configuration, we record the average loss and standard deviation over 10 independent runs.

As before, the best PICNN (partial input convex neural network, [2]) is used as the baseline.

Results are shown in 4 and indicate that the PICKAN achieves accuracy comparable to the best PICNN. The ratio of computational times between PICNN and P1–ICKAN remains consistent with the results reported in 2.2.4.

4 Application for optimal transport

Neural networks that preserve convexity can be used to solve optimal transport problems; see for example [20, 16], which employ ICNNs. In this section, we use ICKANs to solve optimal transport problems and compare their performance with ICNNs.

4.1 Monge optimal transport and Brenier's theorem

Let us consider two probability measures with support $\Omega \subset \mathbb{R}^d$, μ and ν, such that $\int_\Omega \|x\|^2 d\mu(x)$, $\int_\Omega \|x\|^2 d\nu(x) < \infty$. Our goal is to estimate the optimal transport map between X and Y, $T : \Omega \to \Omega$, which is a solution to the Monge problem [22]

$$\inf_{T\#\mu=\nu} \int_\Omega \|x - T(x)\|^2 d\mu(x), \tag{23}$$

where $T\#P(\cdot) := P(T^{-1}(\cdot))$ denotes the pushforward of a measure P, and $\|\cdot\|$ is the Euclidean norm on $\mathbb{R}^d$. Brenier's theorem [5] guarantees existence and uniqueness of the solution to 23, provided that μ is absolutely

Table 4: Testing partial convexity for function in 22 : mean and standard deviation over 10 runs. *NBL* stands for the number of layers, *NBN* the number of neurons, *nbParam* the number of model parameters, while *Time* stands for the time in seconds for one hundred iterations of the stochastic gradient descent.

method	NBL	NBN	P	Average	std	nbParam	Time
Best PICNN	2	80		1.04E-03	7.37E-04	33126	0.28
PICKAN	2	20	20	4.98E-03	1.10E-02	18480	0.77
PICKAN	2	20	40	5.17E-03	4.87E-03	36080	0.77
PICKAN	2	40	20	2.57E-03	3.29E-03	70560	0.78
PICKAN	2	40	40	9.23E-04	5.66E-04	137760	0.78
PICKAN	3	20	20	2.10E-03	3.55E-03	35280	1.10
PICKAN	3	20	40	3.85E-03	3.69E-03	68880	1.10
PICKAN	3	40	20	3.75E-03	5.97E-03	137760	1.11
PICKAN	3	40	40	9.34E-03	1.81E-02	268960	1.11
PICKAN adapt	2	20	20	2.17E-03	2.58E-03	20120	1.05
PICKAN adapt	2	20	40	2.67E-03	4.25E-03	39360	1.05
PICKAN adapt	2	40	20	1.02E-03	1.03E-03	73800	1.06
PICKAN adapt	2	40	40	1.27E-03	1.23E-03	144240	1.06
PICKAN adapt	3	20	20	2.71E-03	3.98E-03	37720	1.48
PICKAN adapt	3	20	40	1.10E-02	1.98E-02	73760	1.48
PICKAN adapt	3	40	20	8.11E-03	1.65E-02	142600	1.49
PICKAN adapt	3	40	40	5.79E-03	5.07E-03	278640	1.49

continuous with respect to the Lebesgue measure, an assumption we make throughout. Furthermore, the optimal transport map can be written as the gradient of a convex function $f : \mathbb{R}^d \to \mathbb{R}$ that is differentiable almost everywhere. Let $CVX(\mu)$ denote the set of convex functions in $L^1(\mu)$. Then f solves

$$\inf_{\varphi \in CVX(\mu)} \int_\Omega \varphi d\mu + \int_\Omega \varphi^\star d\nu,$$

where $\varphi^\star(y) = \sup_{x\in\Omega}\{\langle x, y\rangle - f(x)\}$ for $y \in \Omega$ is the Legendre-Fenchel transform of φ, see [21, Theorem 1]. f is called the Brenier's potential. In [20], it is shown that when ν admits a density, there exists an optimal pair (φ_0, ψ_0) solving

$$\sup_{\substack{\varphi \in CVX(\mu) \\ \varphi^\star \in L^1(\nu)}} \inf_{\psi \in CVX(\nu)} -\int \varphi(x) d\mu(x) - \int \Big(\langle y, \nabla\psi(y)\rangle - \varphi(\nabla\psi(y))\Big) d\nu(y), \tag{24}$$

where $\nabla\psi_0$ is the inverse of the optimal transport map. This formulation enables the use of convex neural networks to approximate both the optimal transport map and its inverse.

4.2 Algorithm

Given samples $X_1, \ldots, X_n \sim \mu$ and $Y_1, \ldots, Y_n \sim \nu$ both identically and independently distributed, the objective is to estimate the optimal transport map between a μ distribution and a ν distribution. We denote by $\hat{\mu}_n = \frac{1}{n}\sum_{i=1}^n \delta_{X_i}$ and $\hat{\nu}_n = \frac{1}{n}\sum_{i=1}^n \delta_{Y_i}$ the empirical distribution of X and Y respectively. In 24, the

potentials φ and ψ are parameterized by two distinct convex neural networks φ_Θ and ψ_θ, which may be either ICKANs or ICNNs, with trainable parameters $\Theta, \theta \in \mathbb{R}^l$.
The empirical counterpart of the minimax problem 24 becomes

$$\max_{\Theta} \min_{\theta} \frac{1}{n} \sum_{i=1}^{n} \varphi_\Theta(\nabla\psi_\theta(Y_i)) - \langle Y_i, \nabla\psi_\theta(Y_i)\rangle - \varphi_\Theta(X_i).$$

We follow the classical minimax optimization scheme described in 1. The network parameter θ is minimized in an inner loop via several gradient-descent steps while the other's Θ is maximized in an outer loop. Since the

Algorithm 1 Minimax algorithm for the transport problem

Require: Batch size n, number of outer iterations I_{ext}, number of inner iteration I_{int}.
  for $i = 1, \dots I_{ext}$ **do**
    for $j = 1, \dots I_{int}$ **do**
      Sample $Y_1, \dots, Y_n \sim \nu$
      $\theta \leftarrow \text{argmin}_\theta \frac{1}{n} \sum_{i=1}^{n} \varphi_\Theta(\nabla\psi_\theta(Y_i)) - \langle Y_i, \nabla\psi_\theta(Y_i)\rangle$ using Adam method
    end for
    Sample $X_1, \dots, X_n \sim \mu$
    Sample $Y_1, \dots, Y_n \sim \nu$
    $\Theta \leftarrow \text{argmax}_\Theta \frac{1}{n} \sum_{i=1}^{n} \varphi_\Theta(\nabla\psi_\theta(Y_i)) - \langle Y_i, \nabla\psi_\theta(Y_i)\rangle - \varphi_\Theta(X_i)$ using Adam method
  end for

ICKAN networks are defined on a compact domain, and because $\nabla\psi(y)$ is not guaranteed to remain within this domain during optimization, the network ψ_θ is linearly extrapolated outside its domain of definition.

4.3 Numerical results on synthetic data

Since the optimal transport map is often unknown in closed form, we construct benchmark problems by choosing μ and a known transport map T and defining $\nu = T\#\mu$. We assess the quality of the estimated map $\hat{T}$ on a validation dataset through the percentage of unexplained variance (UVP) introduced in [16]:

$$\text{UVP}(\%) = 100 \times \frac{\int_\Omega \|T^\star(x) - \hat{T}(x)\|^2 \, d\hat{\mu}_n(x)}{\int_\Omega \|x\|^2 \, d\hat{\nu}_n(x) - \left\| \int_\Omega x \, d\hat{\nu}_n(x) \right\|^2}.$$

A UVP of 100% corresponds to the constant estimator $T^C(x) = \int_\Omega x \, d\hat{\nu}_n(x)$.

As in [16], we use as a benchmark the linear transport map

$$\hat{T}^L(x) = \hat{A}\,(x - \hat{m}_1) + \hat{m}_2,$$

where

$$\hat{m}_1 = \int_\Omega x \, d\hat{\mu}_n(x), \qquad \hat{m}_2 = \int_\Omega x \, d\hat{\nu}_n(x),$$

$$\hat{\Sigma}_1 = \int_\Omega x x^\top \, d\hat{\mu}_n(x) - \hat{m}_1 \hat{m}_1^\top, \qquad \hat{\Sigma}_2 = \int_\Omega x x^\top \, d\hat{\nu}_n(x) - \hat{m}_2 \hat{m}_2^\top,$$

and

$$\hat{A} = \hat{\Sigma}_1^{-1/2} \left(\hat{\Sigma}_1^{1/2} \, \hat{\Sigma}_2 \, \hat{\Sigma}_1^{1/2} \right)^{1/2} \hat{\Sigma}_1^{-1/2}.$$

For the optimization, we use the same hyper-parameters as in [16]:

- $I_{\text{ext}} = 50{,}000$ outer iterations,
- $I_{\text{int}} = 15$ inner iterations,
- batch size equal to 1024,
- learning rate 0.001,
- evaluation every 100 iterations on a test set of size 4,096, and we keep the network with the lowest error,
- validation dataset of size 2^{14}.

For ICKANs, the domain is defined from the minimum and maximum values of a dataset of size 2^{14}. This framework is idealised, as in practice we by no means have this amount of data, and we do not have access to the optimal map used to evaluate the error on the test set. We also initialise the networks with θ_0 minimising $|\nabla f_\theta(x) - x|^2$, so that the map is close to the identity at initialisation.

Transport map of [16] We consider the transport map introduced by Korotin et al. [16]. The authors study the optimal transport map T_1 between a mixture of three Gaussian distributions (μ) and a mixture of ten Gaussians, and similarly T_2 between the same source mixture and another mixture of ten Gaussians. They can then define the optimal transport map $\frac{1}{2}(T_1 + T_2)$. Since T_1 and T_2 are not explicitly known, they learn T_1 and T_2 with an ICNN, $\hat{T}_1$ and $\hat{T}_2$ respectively, that solves the optimal transport problem. The target distribution considered by Korotin et al. [16] and by us is then $\frac{1}{2}\left(\hat{T}_1 + \hat{T}_2\right)\#\mu$. We consider for the ICNN[1] 3 layers with 64, 64 and 32 neurons (same parametrisation as in [16]) and for the ICKANs a network with 2 layers with 64 and 32 neurons or with 10 and 5 neurons. The results are given in 5 for $d \in \{2, 4, 4, 8, 16, 32\}$. Our optimization framework and network parametrization correspond to the [MMv2] case in [16]. For the Cubic-ICKAN with adapted mesh and with 64 and 32 neurons, the errors are much smaller than for the linear map, but can be slightly larger than those obtained by the ICNN parametrization in some case, with similar orders of magnitude. As mentioned in [16], the optimal transport map itself is learned with an ICNN, which can be advantageous for the ICNN parametrisation. Furthermore, we did not search for the optimal parametrisation of the Cubic-ICKAN (nor for the ICNN). The number of mesh points $P \in \{10, 20, 40\}$ does not have much influence on the results, as the use of an unadapted grid does. However, using a P1 mesh instead of a cubic one significantly degrades the results, but the network still outperforms the linear map. Using a smaller network of 10 and 5 neurons for the Cubic-ICKAN results in larger errors, and this difference increases with dimension. The obtained distributions are displayed in 6 for the case $d = 2$ and the Cubic-ICKAN with $P = 10$.

Tensorized case [31] We consider the example in Vacher et al. [31] where the transport map is defined by $T(x) = (T_i(x_i))_{i=1,\dots,d}$ with $T_i(x_i) = x_i + \frac{1}{6-\cos(2\pi x_i)} - 0.2$, $i = 1, \dots, d$,[2] for $x = (x_i)_{i=1,\dots,d} \in [0,1]^d$. μ is a uniform law on $[0,1]^d$. We consider a 3-layers ICNN with 64, 64, 32 neurons and a 2-layers Cubic-ICKAN with $\max(2d, 10)$ and $\max(d, 5)$ neurons, an adapted mesh and $P \in \{10, 20, 40\}$. The results are

[1] We use the implementation at `https://github.com/iamalexkorotin/Wasserstein2Benchmark/`, which uses a CELU activation function.

[2] The example considered is the one from the code `https://github.com/litlboy/OT-Model-Selection/blob/main/Synth-XP/Tensorised/sinkhorn.py` which differs from the one of the paper [31].

Table 5: Percentage of unexplained variance UVP (%) for the linear map, the map parametrized by the Cubic-ICKAN with adapted mesh and $P \in \{10, 20, 40\}$, the Cubic-ICKAN with non adapted mesh and $P = 40$, the P1-ICKAN with adapted mesh and $P = 40$ and the ICNN map when the true map is the one in [16]. For the Cubic-ICKAN, we consider networks with 2 layers and 64 and 32 neurons or 10 and 5 neurons, for the P1-ICKAN 2 layers with 64 and 32 neurons, while for the ICNN we consider 3 layers with 64, 64, and 32 neurons.

Method	Neurons / Dim	2	4	8	16	32
Linear		13.93	14.96	27.29	42.05	55.48
Cubic-ICKAN P=10 adapt	64 32	0.06	0.58	3.00	7.16	9.89
Cubic-ICKAN P=20 adapt	64 32	0.05	0.51	2.44	5.97	7.66
Cubic-ICKAN P=40 adapt	64 32	0.05	0.52	2.82	6.57	5.90
Cubic-ICKAN P=40	64 32	0.06	0.65	3.66	6.63	10.98
P1-ICKAN P=40 adapt	64 32	1.01	6.62	19.99	19.90	27.95
Cubic-ICKAN P=40 adapt	10 5	0.16	1.84	11.56	47.25	101.83
ICNN	64 64 32	0.07	0.27	0.74	1.98	3.01

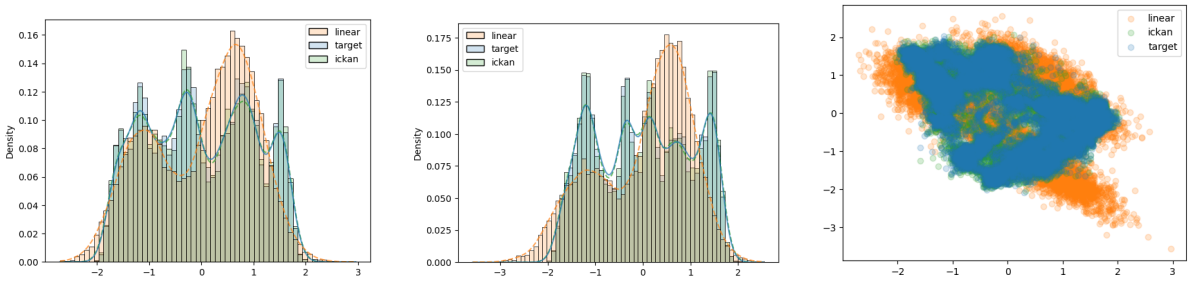

First marginal Second marginal Second versus first

Figure 6: Distribution of the true target distribution as well as the one obtained by linear transport or Cubic-ICKAN transport with adapted mesh, $P = 10$, and 64 and 32 neurons for the map in [16] and $d = 2$. The first two figures include the empirical histogram as well as a Gaussian kernel density estimator with bandwidth selected using Scott's rule [26] (solid line for target, dashed lines for linear and ICKAN transports).

given in 6 for $d \in \{1, 2, 4, 8\}$. The ICNN performs very poorly for $d \in \{4, 8\}$, giving errors of the same order of magnitude as the linear transport map. The Cubic-ICKAN performs very well for all values of P. The obtained distributions are displayed in 7 for the case $d = 2$ case and the Cubic-ICKAN with $P = 10$. We also display in 8 the first component of $\hat{T}\big((x \quad 0.5)^\top\big)$ (0.5 is chosen arbitrarily, the first component of $x_2 \to \hat{T}\big((x \quad x_2)^\top\big)$ being constant and estimating $T_1(x)$), and the second component of $\hat{T}\big((0.5 \quad x)^\top\big)$. We get similar figures for larger dimensions. The neural network reproduces the target distribution and the transport map very well. The better performance of ICKAN over ICNN is probably due to the structure of the Brenier map, which is of the form $f(x) = \sum_{i=1}^d f_i(x_i)$ with $f_i(x_i) = \int_0^{x_i} T_i(s)ds$, $i = 1, \dots, d$: the functions in the Arnold-Kolmogorov representation 3 then have a high degree of smoothness which can lead to a faster rate of convergence, see Proposition 2.2 and 2.3 in [34] in the non-convex case.

Table 6: Percentage of unexplained variance UVP (%) for the linear map, the map parametrized by the Cubic-ICKAN with adapted mesh and $P \in \{10, 20, 40\}$, and the ICNN map and different dimensions when the true map is $T(x) = (T_i(x_i))_{i=1,\dots,d}$ with $T_i(x_i) = x_i + \frac{1}{6-\cos(2\pi x_i)} - 0.2$, $i = 1, \dots, d$.

Method / Dim	1	2	4	8
Linear	0.49	0.54	0.52	0.53
Cubic-ICKAN P=10	0.00	0.01	0.01	0.02
Cubic-ICKAN P=20	0.00	0.02	0.02	0.02
Cubic-ICKAN P=40	0.01	0.02	0.02	0.02
ICNN	0.04	0.05	0.34	0.51

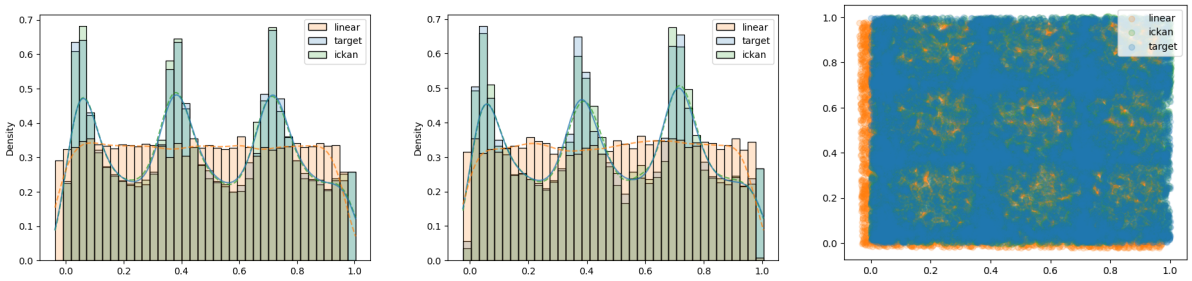

First marginal Second marginal Second versus first

Figure 7: Distribution of the true target distribution as well as the one obtained by linear transport or Cubic-ICKAN transport with adapted mesh and $P = 10$, for the map $T(x) = (T_i(x_i))_{i=1,2}$ with $T_i(x_i) = x_i + \frac{1}{6-\cos(2\pi x_i)} - 0.2$, $i = 1, 2$. The first two figures include the empirical histogram as well as a Gaussian kernel density estimator with bandwidth selected using Scott's rule [26] (solid line for target, dashed lines for linear and ICKAN transports).

Product case We finally consider the map $T = \nabla f$ with f the convex function defined on $[0, 1]^d$ by

$$f(x) = 3^{-d} \prod_{i=1}^{d} \left(x_i^2 + x_i + 1\right), \tag{25}$$

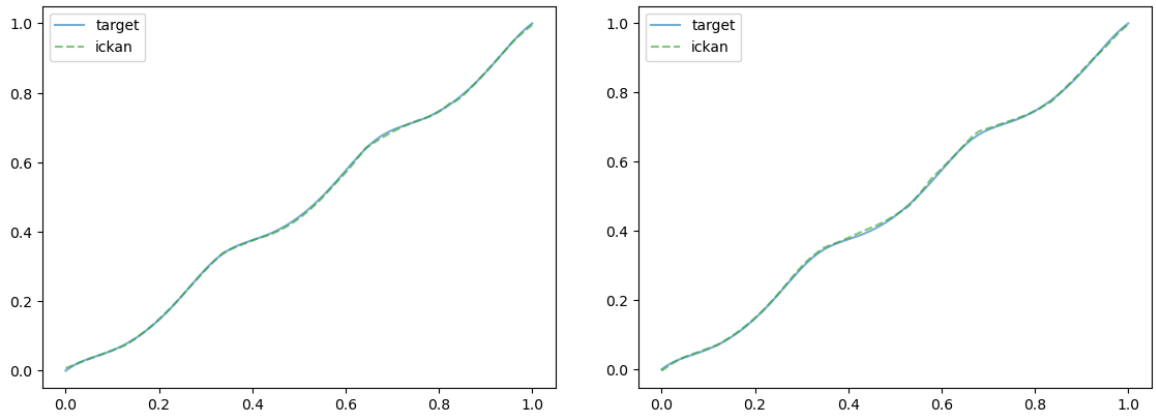

Figure 8: $x \mapsto T_1(x)$ (left) and $x \mapsto T_2(x)$ (right) for the map $T(x) = (T_i(x_i))_{i=1,2}$ with $T_i(x_i) = x_i + \frac{1}{6-\cos(2\pi x_i)} - 0.2$, $i = 1, 2$ as well as the first component of $x \mapsto \hat{T}\left(\begin{pmatrix} x & 0.5 \end{pmatrix}^\top\right)$ (left) and the second component of $x \mapsto \hat{T}\left(\begin{pmatrix} 0.5 & x \end{pmatrix}^\top\right)$ with $\hat{T}$ the estimated map parametrized by the Cubic-ICKAN with adapted mesh and $P = 10$.

and μ is the uniform law on $[0, 1]^d$. The networks have the same architecture as in the second case (tensorized map). The results are given in 7: ICKAN and ICNN give similar results and outperform the linear map benchmark (except for the case $d = 1$ where the optimal transport map is linear).

Table 7: Percentage of unexplained variance UVP (%) for the linear map, the map parametrized by the Cubic-ICKAN with adapted mesh and $P = 40$, and the ICNN map and different dimensions when the true map is $T(x) = \nabla f(x)$ with f given in 25.

Method / Dim	1	2	4	8
Linear	0.00	6.90	16.43	33.57
Cubic-ICKAN P=40	0.01	3.15	2.33	2.85
ICNN	0.00	2.77	1.81	1.30

5 Conclusion

Depending on the case, the new Kolmogorov-Arnold network may outperform the ICNN, though this depends heavily on the case. In particular, its performance varies according to the structure and regularity of the target function. Therefore, this new network may provide an alternative to the ICNN, depending on the structure of the solution. One obvious example is when the solution is separable, as demonstrated in 4.

Additionally, Kolmogorov-Arnold networks are known to be more interpretable than multilayer perceptrons (MLPs) because they are compositions of one-dimensional functions that can easily be plotted, a feature appreciated by users needing to explain the obtained results.

Similarly to the original spline KAN for which the computational cost was highly reduced using an implementation different from the original design[3], more effective implementations of the ICKAN may be possible and are left to future research.

[3] https://github.com/Blealtan/efficient-KAN

References

[1] Akshay Agrawal, Shane Barratt, Stephen Boyd, and Bartolomeo Stellato. Learning convex optimization control policies. In Learning for Dynamics and Control, pages 361–373. PMLR, 2020.

[2] Brandon Amos, Lei Xu, and J Zico Kolter. Input convex neural networks. In International conference on machine learning, pages 146–155. PMLR, 2017.

[3] Gábor Balázs, András György, and Csaba Szepesvári. Near-optimal max-affine estimators for convex regression. In Artificial Intelligence and Statistics, pages 56–64. PMLR, 2015.

[4] Zavareh Bozorgasl and Hao Chen. Wav-Kan: Wavelet Kolmogorov-Arnold Networks. arXiv preprint arXiv:2405.12832, 2024.

[5] Yann Brenier. Polar factorization and monotone rearrangement of vector-valued functions. Communications on pure and applied mathematics, 44(4):375–417, 1991.

[6] Giuseppe C Calafiore, Stephane Gaubert, and Corrado Possieri. Log-sum-exp neural networks and posynomial models for convex and log-log-convex data. IEEE transactions on neural networks and learning systems, 31(3):827–838, 2019.

[7] Yize Chen, Yuanyuan Shi, and Baosen Zhang. Optimal control via neural networks: A convex approach. arXiv preprint arXiv:1805.11835, 2018.

[8] Yize Chen, Yuanyuan Shi, and Baosen Zhang. Input convex neural networks for optimal voltage regulation. arXiv preprint arXiv:2002.08684, 2020.

[9] Robert Demb and David Sprecher. A note on computing with Kolmogorov superpositions without iterations. Neural Networks, 144:438–442, 2021.

[10] Avishek Ghosh, Ashwin Pananjady, Adityanand Guntuboyina, and Kannan Ramchandran. Max-affine regression: Provable, tractable, and near-optimal statistical estimation. arXiv preprint arXiv:1906.09255, 2019.

[11] Avishek Ghosh, Ashwin Pananjady, Adityanand Guntuboyina, and Kannan Ramchandran. Max-affine regression: Parameter estimation for gaussian designs. IEEE Transactions on Information Theory, 68(3):1851–1885, 2021.

[12] Federico Girosi and Tomaso Poggio. Representation properties of networks: Kolmogorov's theorem is irrelevant. Neural Computation, 1(4):465–469, 1989.

[13] Seonho Kim and Kiryung Lee. Max-affine regression via first-order methods. SIAM Journal on Mathematics of Data Science, 6(2):534–552, 2024.

[14] Andrei Nikolaevich Kolmogorov. On the representation of continuous functions of several variables by superpositions of continuous functions of a smaller number of variables. American Mathematical Society, 1961.

[15] Alexander Korotin, Vage Egiazarian, Arip Asadulaev, Alexander Safin, and Evgeny Burnaev. Wasserstein-2 generative networks. arXiv preprint arXiv:1909.13082, 2019.

[16] Alexander Korotin, Lingxiao Li, Aude Genevay, Justin M Solomon, Alexander Filippov, and Evgeny Burnaev. Do neural optimal transport solvers work? A continuous Wasserstein-2 benchmark. Advances in neural information processing systems, 34:14593–14605, 2021.

[17] Věra Kůrková. Kolmogorov's theorem and multilayer neural networks. Neural networks, 5(3):501–506, 1992.

[18] Ziyao Li. Kolmogorov-Arnold Networks are Radial Basis Function Networks. arXiv preprint arXiv:2405.06721, 2024.

[19] Ziming Liu, Yixuan Wang, Sachin Vaidya, Fabian Ruehle, James Halverson, Marin Soljačić, Thomas Y Hou, and Max Tegmark. KAN: Kolmogorov-Arnold Networks. arXiv preprint arXiv:2404.19756, 2024.

[20] Ashok Makkuva, Amirhossein Taghvaei, Sewoong Oh, and Jason Lee. Optimal transport mapping via input convex neural networks. In International Conference on Machine Learning, pages 6672–6681. PMLR, 2020.

[21] Tudor Manole, Sivaraman Balakrishnan, Jonathan Niles-Weed, and Larry Wasserman. Plugin estimation of smooth optimal transport maps. The Annals of Statistics, 52(3):966–998, 2024.

[22] Gaspard Monge. Mémoire sur la théorie des déblais et des remblais. Mem. Math. Phys. Acad. Royale Sci., pages 666–704, 1781.

[23] Subhadip Mukherjee, Sören Dittmer, Zakhar Shumaylov, Sebastian Lunz, Ozan Öktem, and Carola-Bibiane Schönlieb. Learned convex regularizers for inverse problems. arXiv preprint arXiv:2008.02839, 2020.

[24] Tomaso Poggio, Andrzej Banburski, and Qianli Liao. Theoretical issues in deep networks. Proceedings of the National Academy of Sciences, 117(48):30039–30045, 2020.

[25] Maximilian Schaller, Alberto Bemporad, and Stephen Boyd. Learning parametric convex functions. arXiv preprint arXiv:2506.04183, 2025.

[26] David W. Scott and Stephan R. Sain. 9 - Multidimensional Density Estimation. In C.R. Rao, E.J. Wegman, and J.L. Solka, editors, Data Mining and Data Visualization, volume 24 of Handbook of Statistics, pages 229–261. Elsevier, 2005.

[27] S. S. Sidharth, A. R. Keerthana, R. Gokul, and K. P. Anas. Chebyshev polynomial-based Kolmogorov–Arnold networks: An efficient architecture for nonlinear function approximation. arXiv preprint arXiv:2405.07200, 2024.

[28] Lunji Song, Juan Diego Toscano, and Li-Lian Wang. Explicit construction of approximate Kolmogorov-Arnold superpositions with C2-smoothness. arXiv preprint arXiv:2508.04392, 2025.

[29] Hoang-Thang Ta. BSRBF-KAN: A combination of B-splines and Radial Basic Functions in Kolmogorov-Arnold Networks. arXiv preprint arXiv:2406.11173, 2024.

[30] Prakash Thakolkaran, Yaqi Guo, Shivam Saini, Mathias Peirlinck, Benjamin Alheit, and Siddhant Kumar. Can KAN CANs? Input-convex Kolmogorov-Arnold networks (KANs) as hyperelastic constitutive artificial neural networks (CANs). Computer Methods in Applied Mechanics and Engineering, 443:118089, 2025.

[31] Adrien Vacher and François-Xavier Vialard. Parameter tuning and model selection in optimal transport with semi-dual Brenier formulation. Advances in Neural Information Processing Systems, 35:23098–23108, 2022.

[32] Xavier Warin. Some non-monotone schemes for time dependent hamilton–jacobi–bellman equations in stochastic control. Journal of Scientific Computing, 66(3):1122–1147, 2016.

[33] Xavier Warin. The GroupMax neural network approximation of convex functions. IEEE Transactions on Neural Networks and Learning Systems, 2023.

[34] Xavier Warin. P1-KAN: an effective Kolmogorov-Arnold Network with application to hydraulic valley optimization. arXiv preprint arXiv:2410.03801, 2024.

A One dimensional approximation with one layer

For the P1-ICKAN and the Cubic-ICKAN, we illustrate how a single layer can effectively approximate various one-dimensional convex functions using adaptation.

A.1 Using P1-ICKAN

As an example, it is possible to minimize the mean squared error of a one dimensional convex function with its approximation 4-6 by training $b, \hat{b}, (d_i)_{i=1,\dots,P-1}$, and $(e_i)_{i=1,\dots,P}$. With θ the vector of parameters to be trained, our approximation $\tilde{f}^\theta$ of a function f is parametrized by θ and we minimize

$$\mathbb{E}[(f(X) - \tilde{f}^\theta(X))^2]$$

where X is a random variable sampled uniformly on $[-10, 10]$. We give the results approximating the functions f_i, $i = 1, \dots, 4$ on 9 where

1. $f_1(x) = x^2$,
2. $f_2(x) = x^2 + 10[(e^x - 1)1_{x<0} + x1_{x\geq 0}]$,
3. $f_3(x) = (|x|^2 + 1)^2$,
4. $f_4(x) = |x|1_{|x|\leq 3} + \frac{x^2-3}{2}$.

The plots are obtained adapting the grid with $P = 10$ or $P = 20$. We also plot the adapted vertices.

A.2 Cubic-ICKAN

As for the piecewise linear approximation, we provide on 10 the vertices and an estimation obtained by adapting the grid with $P = 5$ or $P = 10$.

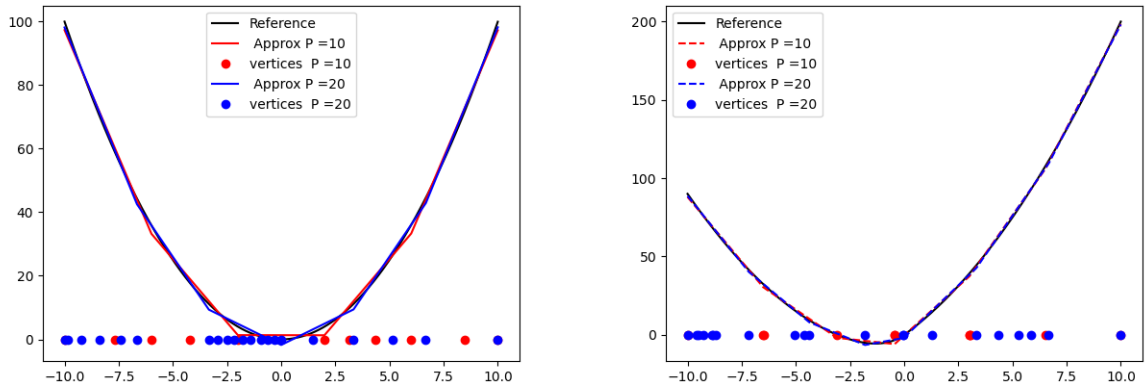

f_1 f_2

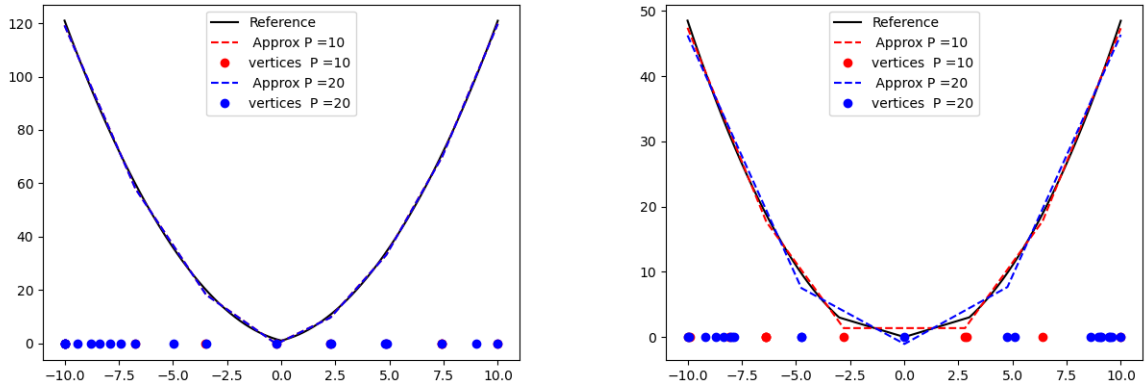

f_3 f_4

Figure 9: Piecewise linear approximation of a one dimensional function using 4- 6 with adaptation.

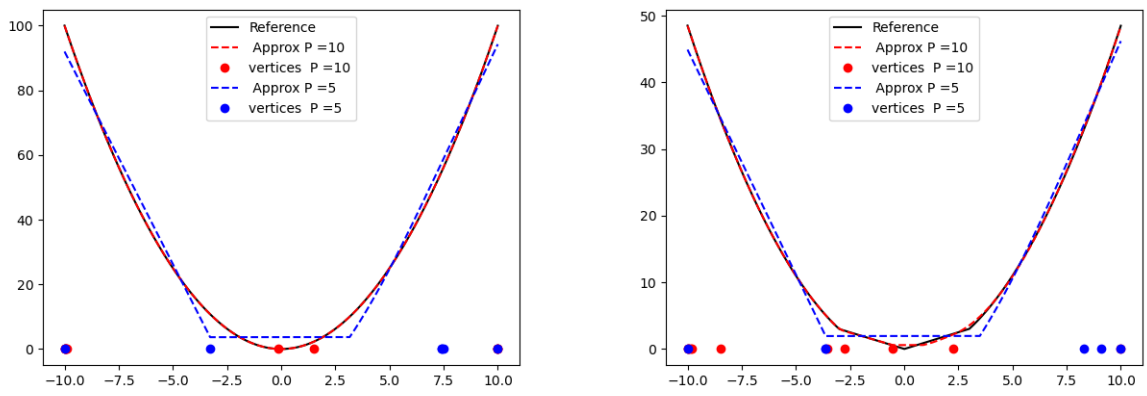

f_1 f_4

Figure 10: Cubic spline approximation of a one dimensional function using 8- 9 with adaptation.

B Proof of 2.1 and 2.2

B.1 Proof of 2.1

The proof is constructive and is based on the proof of theorem 1 in [7]. One wants to approximate a Lipschitz convex function on $[0,1]^n$ denoted f by a P1-ICKAN network with adaptation. First any Lipschitz convex function on $[0,1]^n$ can be approximated within ϵ by the maximum of a finite set of affine functions (Lemma 1 in [7] or Proposition 1 in [33]), that is for any $\epsilon > 0$, there exists $N \geq 1$ and a function f_N such that $|f(x) - f_N(x)| < \epsilon$ for any $x \in [0,1]^n$, with a representation

$$f_N(x) := \max(\alpha_1^\top x + \beta_1, \ldots, \alpha_N^\top x + \beta_N),\ \alpha_i \in \mathbb{R}^n,\ \beta_i \in \mathbb{R},\ i = 1, \ldots, N. \tag{26}$$

As a consequence, the proof of 2.1 boils down to show that the P1-ICKAN network with adaptation can represent any maximum of a finite set of affine functions of type 26 for any $N \geq 1$.

Following [7], we start by the case $N = 2$ and begin to show that the linear KAN can represent the maximum of two affine functions, that is any function of the form f_2. First, we have for $x \in [0,1]^n$, $\alpha_i \in \mathbb{R}^n$, $\beta_i \in \mathbb{R}$, $i = 1, 2$,

$$f_2(x) = \max((\alpha_1^\top - \alpha_2^\top)x + \beta_1 - \beta_2, 0) + \alpha_2^\top x + \beta_2. \tag{27}$$

We consider $P = 2$ and a $L = 3$-layers neural network to match 27 with $n_1 = 3$ neurons for the first layer and $n_2 = 2$ neurons for the second layer. For the first layer, we consider the lattice defined by $\hat{x}_{0,j,0} = 0$, $\hat{x}_{0,j,1} = \frac{1}{2}$, and $\hat{x}_{0,j,2} = 1$, $1 \leq j \leq n$, and we define in 10 the parameters

$$
\begin{aligned}
b_{0,1,1} &= \beta_1,\\
b_{0,1,j} &= 0 \text{ for } 1 < j \leq n,\\
\hat{b}_{0,1,j} &= \alpha_{1,j} \text{ for } 1 \leq j \leq n,\\
d_{0,1,j,1} &= 0 \text{ for } 1 \leq j \leq n,\\
b_{0,2,1} &= -\beta_2,\\
b_{0,2,j} &= 0 \text{ for } 1 < j \leq n,\\
\hat{b}_{0,2,j} &= -\alpha_{2,j} \text{ for } 1 \leq j \leq n,\\
d_{0,2,j,1} &= 0 \text{ for } 1 \leq j \leq n,\\
b_{0,3,1} &= \beta_2,\\
b_{0,3,j} &= 0 \text{ for } 1 < j \leq n,\\
\hat{b}_{0,3,j} &= \alpha_{2,j} \text{ for } 1 \leq j \leq n,\\
d_{0,3,j,1} &= 0 \text{ for } 1 \leq j \leq n.
\end{aligned}
\tag{28}
$$

One checks that the output of the first layer is given by

$$
\begin{aligned}
\hat{\kappa}^0_{n,n_1}(x,[0,1]^n)_1 &= \alpha_1^\top x + \beta_1,\\
\hat{\kappa}^0_{n,n_1}(x,[0,1]^n)_2 &= -\alpha_2^\top x - \beta_2,\\
\hat{\kappa}^0_{n,n_1}(x,[0,1]^n)_3 &= \alpha_2^\top x + \beta_2.
\end{aligned}
$$

For the second layer, we have $n_2 = 2$ neurons. Let $I_1 = \prod_{j=1}^{3}[\hat{x}_{1,j,0}, \hat{x}_{1,j,2}]$ denote the image of $[0,1]^n$ by the first layer and consider for each $j = 1,2,3$ any $\hat{x}_{1,j,1} \in]\hat{x}_{1,j,0}, \hat{x}_{1,j,2}[$ to define the grid $\mathcal{G}^1$. For the first neuron, we consider the parameters

$$
\begin{aligned}
&b_{1,1,j} = \hat{x}_{1,j,0},\ j = 1,2,\\
&\hat{b}_{1,1,j} = 1,\ j = 1,2,\\
&d_{1,1,j,1} = 0,\ j = 1,2,\\
&b_{1,1,3} = 0,\\
&\hat{b}_{1,1,3} = 0,\\
&d_{1,1,3,1} = 0
\end{aligned}
$$

in order to get

$$
\hat{\kappa}^1_{n_1,n_2}(x,\mathcal{G}_1)_1 = x_1 + x_2.
$$

In the same way, for the second neuron, we consider the parameters

$$\begin{aligned}
&b_{1,2,j} = 0,\ j = 1, 2,\\
&\hat{b}_{1,2,j} = 0,\ j = 1, 2,\\
&d_{1,2,j,1} = 0,\ j = 1, 2,\\
&b_{1,2,3} = \hat{x}_{1,3,0},\\
&\hat{b}_{1,2,3} = 1,\\
&d_{1,2,3,1} = 0
\end{aligned}$$

to get

$$\hat{\kappa}^1_{n_1,n_2}(x, \mathcal{G}_1)_2 = x_3.$$

At this stage, we then have as output of the two first layers

$$\begin{aligned}
\hat{\kappa}^1_{n_1,n_2} \circ \kappa^0_{n,n_1}(x, [0,1]^n)_1 &= (\alpha_1^\top - \alpha_2^\top)x + \beta_1 - \beta_2,\\
\hat{\kappa}^1_{n_1,n_2} \circ \kappa^0_{n,n_2}(x, [0,1]^n)_2 &= \alpha_2^\top x + \beta_2.
\end{aligned}$$

Let $I_2 = \prod_{j=1}^{2} [\hat{x}_{2,j,0}, \hat{x}_{2,j,2}]$ denote the image of $\mathcal{G}_1$ by the second layer. For the third layer, we first consider the case where the non linearity is active for the first component of the second layer output $\hat{\kappa}^1_{n_1,n_2} \circ \kappa^0_{n,n_1}(x, [0,1]^n)_1$, that is $0 \in]\hat{x}_{2,1,0}, \hat{x}_{2,1,2}[$ (only depending on the function that we try to equalize, f_2). In this case, we take $\hat{x}_{2,1,1} = 0 \in]\hat{x}_{2,1,0}, \hat{x}_{2,1,2}[$, and any $\hat{x}_{2,2,1} \in]\hat{x}_{2,2,0}, \hat{x}_{2,2,2}[$ to construct $\mathcal{G}_2$, and define

$$\begin{aligned}
&b_{2,1,1} = 0,\\
&\hat{b}_{2,1,1} = 0,\\
&d_{2,1,1,1} = 1,\\
&b_{2,1,2} = \hat{x}_{2,2,0},\\
&\hat{b}_{2,1,2} = 1,\\
&d_{2,1,2,1} = 0.
\end{aligned} \tag{29}$$

The three first lines in 29 define the ReLU with an active non linearity, while the three last define the identity function. We thus get the desired result

$$\hat{\kappa}^1_{n_2,1} \circ \kappa^1_{n_1,n_2} \circ \kappa^0_{n,n_1}(x, [0,1]^n)_1 = \max((\alpha_1^\top - \alpha_2^\top)x + \beta_1 - \beta_2, 0) + \alpha_2^\top x + \beta_2$$

equal to $f_2(x)$ from 27. Now consider the case when the non linearity is not active. It is enough to take for the lattice any $\hat{x}_{2,1,1} \in]\hat{x}_{2,1,0}, \hat{x}_{2,1,2}[$ and to replace $b_{2,1,1}$, $\hat{b}_{2,1,1}$, and $d_{2,1,1,1}$ in 29 by

$$\begin{aligned}
&b_{2,1,1} = \hat{x}_{2,1,0},\\
&\hat{b}_{2,1,1} = 1,\\
&d_{2,1,1,1} = 0
\end{aligned}$$

to obtain the identity function.

Similarly as in [7], one can extend iteratively the procedure for a given N using

$$f_N(x) = \max(f_{N-1}(x) - (\alpha_N^\top x + \beta_N), 0) + \alpha_N^\top x + \beta_N). \tag{30}$$

If one has constructed $f_{N-1}(x)$, add

- Two neurons at the end of the first layer, with outputs $-\alpha_N^\top x - \beta_N$ and $\alpha_N^\top x + \beta_N$, in the same way as the last two neurons in the first layer in the case $N = 2$,
- Two neurons at the end of each existing layer, that output exactly the outputs of the two last neurons of the previous layer, in the same way that the last neuron in the second layer in the case $N = 2$, and we get $-\alpha_N^\top x - \beta_N$ and $\alpha_N^\top x + \beta_N$ for the outputs of the two last neurons of the last layer.

From this, we get a third dimensional output corresponding to $f_{N-1}(x)$, $-\alpha_N^\top x - \beta_N$ and $\alpha_N^\top x + \beta_N$. The situation is exactly the same as for the case $N = 2$, after that the first layer has been constructed. It remains to add the two layers similar to the two last layers in the case $N = 2$ to get the desired output 30.

remark B.1 *The first layer outputs $-\alpha_N^\top x - \beta_N$ in order to avoid to have negative values of $\hat{b}_{l,k,j}$ in the other layers which, contrarily to the first layer, consider $\max(\hat{b}_{l,k,j}, 0)$ and not $\hat{b}_{l,k,j}$. This is similar to the duplication trick in the proof of theorem 1 in [7].*

B.2 Proof of 2.2

The idea of the proof is the same as in the adapted case. The main difference is that, without mesh adaptation, we must control the approximation error by increasing the number of mesh points P.

For simplicity, we allow here the number of mesh points $P + 1$ to vary from one neuron to another. This has no impact because a neuron with a mesh size of $M + 1$ is a special case of a neuron with a mesh size of $P + 1$ if $M \leq P$.

We first consider the case $N = 2$ as in the adapted proof. The construction of the first two layers is identical. The only difference appears in the third layer, when the nonlinearity is active, a priori

$$0 \notin]\hat{x}_{2,1,0}, \hat{x}_{2,1,2}[$$

and the ReLU function must be approximated even though. For the first neuron of this layer, given P, there exists k such that

$$|\hat{x}_{2,1,k}| \leq \frac{\hat{x}_{2,1,P} - \hat{x}_{2,1,0}}{P}.$$

We then choose parameters

$$\begin{aligned}
&b_{2,1,1} = 0,\\
&\hat{b}_{2,1,1} = 0,\\
&d_{2,1,1,i} = 0, \text{ for } i \neq k\\
&d_{2,1,1,k} = 1
\end{aligned}$$

and we keep $P = 2$ for the second neuron and parameters

$$\begin{aligned}
&b_{2,1,2} = \hat{x}_{2,2,0},\\
&\hat{b}_{2,1,2} = 1,\\
&d_{2,1,2,1} = 0.
\end{aligned}$$

The output of the neural network is then

$$\begin{aligned}\kappa_2(x) &:= \hat{\kappa}^1_{n_2,1} \circ \kappa^1_{n_1,n_2} \circ \kappa^0_{n,n_1}(x, [0,1]^n)_1 \\ &= \max((\alpha_1^\top - \alpha_2^\top)x + \beta_1 - \beta_2 - \hat{x}_{2,1,k}, 0) + \alpha_2^\top x + \beta_2\end{aligned}$$

so that

$$|f_2(x) - \kappa_2(x)| \leq |\hat{x}_{2,1,k}| \leq \frac{C_2}{P}.$$

The previous result can be extended to the general case $N \geq 2$ so that our network representation κ_N is such that

$$|f_N(x) - \kappa_N(x)| \leq \frac{C_N}{P}$$

and

$$|f(x) - \kappa_N(x)| \leq \frac{C_N}{P} + \epsilon.$$

Therefore, setting P equal to the integer part of $\frac{C_N}{\epsilon} + 1$ provides a 2ϵ approximation of f.